A Giant Impact Origin for the First Subduction on Earth

Qian Yuan^{1,2*}, Michael Gurnis², Paul Asmiow¹, Yida Li²

Affiliations:

5

10

15

20

25

30

35

40

¹Division of Geological and Planetary Sciences, California Institute of Technology, Pasadena, California CA 91125, USA

²Seismological Laboratory, California Institute of Technology, Pasadena, CA 91125, USA

*Correspondence to: qyuan@caltech.edu

Abstract: Hadean zircon grains provide a potential record of Earth's earliest subduction around 4.3 billion years ago. However, it remains enigmatic how subduction could be initiated so shortly after the presumably final assemblage stage of Earth, the Moon-forming giant impact (MGI). Recent work indicates that Earth's lower half-mantle remains mostly solid after this impact and parts of the impactor's mantle may conserve as the two seismically-observed large low-shear velocity provinces (LLSVPs). Here, we show that strong mantle plumes rising from the LLSVPs can induce subduction initiation ~200 Myr after the MGI. Our 2D and 3D thermomechanical simulations demonstrate that the hot core-mantle boundary temperature and relatively weak lithosphere after the impact are key factors to trigger such an early subduction. Our model links the earliest subduction with the MGI, and has implications for understanding the diverse tectonic regimes of rocky planets.

One Sentence Summary: The consequence of Moon-forming giant impact can give rise to the first subduction on Earth in the early Hadean.

Main Text:

As planetary exploration continues, Earth emerges with a so far unique signature: plate tectonics. In plate tectonics, subduction is the major process affecting the geodynamic and geochemical evolution of our planet, but how the first subduction started remains enigmatic and contentious. Although debated (1), analyses of Hadean detrital zircons show geochemical signals consistent with subduction as early as 4.3 Ga (2, 3). Thus, the earliest subduction may occur less than ~200 million years after the main stage of Earth's formation, which is widely believed to be ended with the Moon-forming giant impact (MGI) (4). The collision of a protoplanet called Theia with the proto-Earth at ~4.51 Ga is expected to largely reset the initial physical and chemical conditions of Earth's evolution, but a critical—but often neglected—effect on its lasting influence on Earth's tectonic evolution has not been explored quantitatively. Here we propose that the conditions set by a canonical MGI creates favorable conditions for the initiation of subduction in Earth's earliest period, thereby exemplifying the pivotal influence of initial condition set by giant impact processes on the tectonic evolution of terrestrial planets.

A number of mechanisms have been proposed to initiate the early subduction (5), but among them only two do not need a pre-existing weakness in the lithosphere that is required in most of these models. Those mechanisms are impact-driven (6) and plume-induced (7, 8) subduction initiation. The impact-driven hypothesis is only likely during the Late Heavy Bombardment (4.1-

3.8 Ga), too late to explain the Hadean detrital zircons record. Thus, plume-induced subduction stands as a more favorable candidate for nucleating the earliest subduction process. However, it is unclear how to generate the required strong mantle plumes in the hot Hadean mantle. Recent highresolution MGI simulations show that Earth's lower half-mantle remains largely solid after the impact (9, 10) and our previous study indicates that some Fe-rich (11) and dense Theia mantle materials are candidates for a chemical origin of the two seismically-observed large low-shear velocity provinces (LLSVPs) (12), which are commonly associated with strong mantle plumes, large igneous provinces, and intense hotspot volcanisms (13, 14). Here, we formulated 2-D and 3-D whole-mantle thermomechanical models with visco-elasto-plastic rock rheology (see Methods) to test the hypothesis that strong mantle plumes can arise from LLSVPs, weaken the lithosphere and eventually cause subduction initiation (Fig. 1). If LLSVPs are primordial (14, 15), we argue that their associated mantle plumes may help generate sporadic subduction events until subduction becomes self-organized as lithosphere gets cooler and stronger. After that time, the cold and strong lithosphere would inhibit further plume-induced subduction. Our model provides a hitherto unrecognized link between the incipient subduction and the Moon's formation, and underscores the importance of the early planetary accretion in shaping the planet's subsequent evolution.

5

10

15

20

25

30

35

40

45

Following the MGI, a certain depth of magma ocean at surface is expected. Modelling magma ocean solidification is beyond the scope of this paper, and we note it is generally accepted the solidification process should mostly complete within 100 Myr, depending on volatile content (16). For simplicity, we perform post-magma ocean mantle convection models to simulate the subsequent dynamics 100 Myr from the MGI given the mantle already solidified with a protolithosphere. Our 2D reference thermomechanical model consists of an intrinsically dense layer of LLSVP materials and a proto-lithosphere with a prescribed age of 50 Ma from half-space-cooling model. Current estimates of the present-day core-mantle boundary (CMB) temperature ranges from 2,500 K to 4,500 K (17), but because of Earth's secular cooling, the Hadean CMB temperature should be higher, which is also consistent with the observation that the CMB temperature was increased the most due to the accumulation of Theia's core materials that was most severely heated during the MGI (18). We therefore use a higher CMB temperature (5,273 K) for most cases and the initial LLSVP temperature is set as 1,273 K lower than the CMB. Such high CMB temperature may lead to partial melting of the overlying LLSVP materials and lower mantle materials, but the melting extent may not be complete given the high melting temperatures of lower mantle minerals (19, 20) and we also validated our results with lower CMB temperatures (4,273 and 3,273 K). The yield strength of the lithosphere in Hadean is expected to be low owing to the hotter thermal structure relative to the present-day (21), and we mostly used a 40 MPa yield strength for the proto-lithosphere. All parameters are listed in table S1.

Figure 2 shows a reference model where a mantle plume from the LLSVP-like thermochemical piles ruptures the lithosphere and initiates subduction after ~150 Myr. The initial layer of the thermochemical piles starts to form individual piles due to a combination of strong CMB heating and its depth-dependent density (see Methods). Meanwhile, the lithosphere grows thicker due to inefficient cooling while in a stagnant lid mode of convection. At 127 Myr, a strong mantle plume develops from the top of the central pile (Fig. 2A). This mantle plume quickly rises to the upper mantle, becoming narrower due to the viscosity decrease at the transition zone. As the plume approaching the surface, the lithosphere is locally weakened above the plume, and at 138 Myr, the

persistent localized thinning resulting from the plume eventually leads to its penetration of the lithosphere, forming a plume wedge that incises through the lithosphere (Fig. 2C). Meanwhile, the associated lithospheric thickening around the plume head results in two lithospheric-scale shear bands in each side of the plume head (Fig. 2C). Following this, the plume starts to spread at the surface, overcoming the yield strength of the surrounding lithosphere segments and eventually forming shear zones along the subducting plate boundary that promotes self-sustaining and retreating subduction at 141 Myr (Fig. 2D). As slabs continues to subduct deeper, a portion of the subducted crust eventually reached temperature higher than 1,073 K, which allows its partial melting to form buoyant melts that can form the early felsic rocks indicated by geological records.

10

15

20

25

5

Compared to the reference case, the time to initiate subduction is 10 Myr longer when the yield strength of the lithosphere is increased from 40 to 70 MPa (Fig. 3A). When the lithosphere yield stress is further increased to 100 MPa, close to present-day (>100-150 MPa) (22), as expected the plume is not capable of penetrating through the lithosphere to induce subduction, but spreads at the base of lithosphere (Fig. 3B). The CMB temperature can significantly influence the buoyancy and instability of LLSVPs and associated mantle plumes, but its exact value in the Hadean is not known, although presumably it should be higher than the present. We decreased the CMB temperature used in reference case to 4,273 K (Fig. 3C) and 2,773 K (Fig. 3D) respectively in two cases, and find that the higher the CMB temperature, the easier and faster for the plume to induce subduction. In the case with the 2,773 K CMB temperature, subduction is marginally initiated at a much late time (579 Myr) (Fig. 3D), however, even if the lithosphere yield strength is slightly increased from 40 MPa to 45 MPa, no subduction is initiated with this low CMB temperature (Fig. 3E). We also considered the possibility of higher mantle temperatures during the Hadean, and find the hotter mantle temperature allows the plume from LLSVP to rise faster and induce subduction ~30 Myr earlier than the reference (Fig. 3F). Different rheological properties are additionally tested, such as smaller viscosity of the LLSVPs (Fig. 3G), larger reference viscosity (Fig. 3H), higher temperature-dependent viscosity (fig. S1A). These computations show that the larger the viscosity of the model, the longer it takes for plumes to induce subduction.

30

35

We tested cases with different density structures. As described above, we performed a case with a basaltic crust that is chemical-buoyant (fig. S1B), and find overall dynamics closely resemble those of the reference case. We also varied the density and initial temperature of the LLSVP materials, such as a relatively less dense LLSVP materials (fig. S1C), a lower initial temperature of LLSVPs (fig. S1D), and find the results are overall similar to the reference model. By varying ages of the lithosphere (fig. S2), our experiments revealed that when the lithosphere is younger than 30 Myr, it is challenging for plumes to induce subduction (fig. S2A) as the thickened young lithosphere cannot provide a large slab pull force to exceed its yield strength. We also tested different weakening rates, finding they mainly affect the shear zone's thickness and location, with minor influence on the model results (fig. S3). Models with higher resolution (fig. S4A), different aspect ratio (5:1) with either free-slip (fig. S4B) or periodic boundary conditions (fig. S4C) do not significantly affect our results.

40

45

To further validate our 2D results, we performed 3D whole-mantle thermomechanical models also using the same *Underworld2* code (23). Our 3D reference case has the exactly same model parameters setup as the 2D reference model except being three-dimensional. Similar to the 2D models, we observe that a strong mantle plume can be generated from the top of LLSVP-like piles

(Fig. 4A-B). As the plume rises and pierces through a lithosphere (Fig. 4B), it starts to spread atop of the broken segments of the lithosphere within the circular sector-like region, and pushes the lithosphere segment downward into the mantle by overcoming the yield strength of the lithosphere. As the plume continues to spread, the surface shear zones extends to a deeper depth along the subducting plate boundary which facilitates the subduction and retreat of the circular sector-like subduction zones (Fig. 4D), resembling previous 3D results (8). In another 3D case we find a slightly higher yield strength of the lithosphere (60 MPa) does not significantly affect the results (fig. S5). However, for a 3D case with a lower CMB temperature, 4,273 K, plume does not penetrate the thick lithosphere to initiate subduction (fig. S6). Thus, the observations we identified in 2D computations that a higher CMB temperature and lower lithosphere strength facilitate plume-induced subduction remain valid in 3D, though the threshold values may differ due to effect of geometry and plume size and morphology. We further compared our 3D results to corresponding 2D model, and the results show a limited boundary effect in affecting the feasibility of plume-induced subduction initiation in 3D (fig. S7).

Hadean detrital zircons and short-lived radioactive isotopes anomalies support the notion of operation of subduction in the Hadean (2, 3, 24). But how subduction could be initiated from an intact lithosphere without weakness remains perplexing. One study suggests subduction can start rapidly after mantle solidification from a magma ocean (25), but their drip-like downwellings contradicts recent inference on modern subduction settings responsible for the equilibrium melts of Hadean zircons in Jack Hills (26). Other previous studies often assume a presence of surface oceans in the early Hadean, which is argued to have the capacity to thermally weaken the stiff lithosphere to initiate subduction (27). However, the mechanisms to introduce water into oceanic lithosphere down to the depth of a few tens of kilometers remain debated. Plume-induced subduction is an appealing mechanism that does not require pre-existing weak zones or other external forces (28), but developing such strong mantle plumes in an expected hot Hadean Earth is difficult. Given the close proximity of these earliest records to the initial condition of Earth established by the presumed MGI, it is vital to investigate its potential influence on the feasibility of subduction initiation.

Using novel and high-resolution MGI simulation, recent studies show Earth's lower half-mantle remains mostly solid (9) and a portion of Theia's iron-rich mantle can sink and form the seismically-observed LLSVPs (12), which are commonly associated with large igneous provinces and hotspot volcanisms (13). Our simulations here show that strong mantle plumes from the LLSVPs can naturally rise to trigger subductions in the early Hadean, consistent with geological observations. We quantitatively tested how our results are influenced by the strength and age of the lithosphere, CMB temperature, weakening rate, rheology and density structure, model geometry (2D and 3D). These computations consistently show plumes from LLSVPs are capable of breaking the expected weak proto-lithosphere to induce subduction when the CMB temperature is high in the Hadean. The results of our 2D and 3D numerical experiments agree with previous plume-induced subduction models (8). To our knowledge, we present the first self-consistent dynamic model with LLSVP-sourced plumes that induce subduction in a stagnant lid convection state. After the initial heat burst due to a hotter CMB after the MGI, plume may not be strong enough to induce new subductions (Fig. 3E), but if LLSVP materials are enriched in heat-generating elements (29), LLSVP-sourced plumes would be poised to trigger transient episodes of

new subductions (fig. S8) until subduction becomes self-organized when Earth gets cooler and lithosphere becomes stronger, which is required for the onset of plate tectonics.

Unraveling the origins of diversity among terrestrial planets is a fundamental goal in Earth and planetary science. The earliest phase of planetary evolution is dictated by the giant impact stage which provides the initial conditions for planetary evolution (30). Our study here provides a hitherto unrecognized geodynamic effect on subduction initiation from the consequence of the MGI, which may have implication for understanding the evolutionary dichotomy between Earth and Venus given the absence of moon and also plate tectonics on Venus.

References and Notes:

5

10

15

25

- 1. A. I. S. Kemp, S. A. Wilde, C. J. Hawkesworth, C. D. Coath, A. Nemchin, R. T. Pidgeon, J. D. Vervoort, S. A. DuFrane, Hadean crustal evolution revisited: New constraints from Pb–Hf isotope systematics of the Jack Hills zircons. *Earth and Planetary Science Letters*. **296**, 45–56 (2010).
- 2. J. W. Valley, W. H. Peck, E. M. King, S. A. Wilde, A cool early Earth. *Geology*. **30**, 351–354 (2002).
- 3. E. B. Watson, T. M. Harrison, Zircon thermometer reveals minimum melting conditions on earliest earth. *Science*. **308**, 841–844 (2005).
- 4. R. M. Canup, E. Asphaug, Origin of the Moon in a giant impact near the end of the Earth's formation. *Nature*. **412**, 708–712 (2001).
 - 5. R. J. Stern, T. Gerya, Subduction initiation in nature and models: A review. *Tectonophysics*. **746**, 173–198 (2018).
 - 6. C. O'Neill, S. Marchi, S. Zhang, W. Bottke, Impact-driven subduction on the Hadean Earth. *Nature Geoscience.* **10**, 793–797 (2017).
 - 7. K. Ueda, T. Gerya, S. V. Sobolev, Subduction initiation by thermal—chemical plumes: Numerical studies. *Physics of the Earth and Planetary Interiors*. **171**, 296–312 (2008).
 - 8. T. V. Gerya, R. J. Stern, M. Baes, S. V. Sobolev, S. A. Whattam, Plate tectonics on the Earth triggered by plume-induced subduction initiation. *Nature*. **527**, 221–225 (2015).
- 9. H. Deng, M. D. Ballmer, C. Reinhardt, M. M. M. Meier, L. Mayer, J. Stadel, F. Benitez, Primordial Earth Mantle Heterogeneity Caused by the Moon-forming Giant Impact? *The Astrophysical Journal.* **887**, 211 (2019).
 - 10. H. Deng, C. Reinhardt, F. Benitez, L. Mayer, J. Stadel, A. C. Barr, Enhanced Mixing in Giant Impact Simulations with a New Lagrangian Method. *The Astrophysical Journal.* **870**, 127 (2019).

- 11. M. M. M. Meier, A. Reufer, R. Wieler, On the origin and composition of Theia: Constraints from new models of the Giant Impact. *Icarus.* **242**, 316–328 (2014).
- 12. Q. Yuan, M. Li, B. Ko, S. Desch, Giant Impact Origin for the Large Low Shear Velocity Provinces. *52nd Lunar and Planetary Science Conference 2021*. **2021**, 1980–1981 (2021).
- 5 13. T. H. Torsvik, K. Burke, B. Steinberger, S. J. Webb, L. D. Ashwal, Diamonds sampled by plumes from the core-mantle boundary. *Nature*. **466**, 352–355 (2010).

15

- 14. A. K. McNamara, A review of large low shear velocity provinces and ultra low velocity zones. *Tectonophysics*. **760**, 199–220 (2019).
- 15. S. Mukhopadhyay, Early differentiation and volatile accretion recorded in deep-mantle neon and xenon. *Nature*. **486**, 101–104 (2012).
- 16. L. T. Elkins-Tanton, Linked magma ocean solidification and atmospheric growth for Earth and Mars. *Earth and Planetary Science Letters*. **271**, 181–191 (2008).
- 17. F. Deschamps, L. Cobden, Estimating core-mantle boundary temperature from seismic shear velocity and attenuation. *Front. Earth Sci.* **10**, 1031507 (2022).
- 18. R. M. Canup, Simulations of a late lunar-forming impact. *Icarus*. **168**, 433–456 (2004).
 - 19. A. Zerr, R. Boehier, Melting of (Mg, Fe)SiO₃ -Perovskite to 625 Kilobars: Indication of a High Melting Temperature in the Lower Mantle. *Science*. **262**, 553–555 (1993).
 - 20. G. Shen, P. Lazor, Measurement of melting temperatures of some minerals under lower mantle pressures. *J. Geophys. Res.* **100**, 17699–17713 (1995).
- 21. P. M. Gunawardana, G. Morra, P. Chowdhury, P. A. Cawood, Calibrating the Yield Strength of Archean Lithosphere Based on the Volume of Tonalite-Trondhjemite-Granodiorite Crust. *Front. Earth Sci.* **8**, 548724 (2020).
 - 22. D. L. Kohlstedt, B. Evans, S. J. Mackwell, Strength of the lithosphere: Constraints imposed by laboratory experiments. *J. Geophys. Res.* **100**, 17587–17602 (1995).
- 23. J. Mansour, J. Giordani, L. Moresi, R. Beucher, O. Kaluza, M. Velic, R. Farrington, S. Quenette, A. Beall, Underworld2: Python Geodynamics Modelling for Desktop, HPC and Cloud. *JOSS*. **5**, 1797 (2020).
 - 24. E. Hyung, S. B. Jacobsen, The ¹⁴² Nd/ ¹⁴⁴ Nd variations in mantle-derived rocks provide constraints on the stirring rate of the mantle from the Hadean to the present. *Proc. Natl. Acad. Sci. U.S.A.* **117**, 14738–14744 (2020).
 - 25. B. J. Foley, D. Bercovici, L. T. Elkins-Tanton, Initiation of plate tectonics from post-magma ocean thermochemical convection. *J. Geophys. Res. Solid Earth.* **119**, 8538–8561 (2014).

- 26. S. Turner, S. Wilde, G. Wörner, B. Schaefer, Y.-J. Lai, An andesitic source for Jack Hills zircon supports onset of plate tectonics in the Hadean. *Nat Commun.* **11**, 1241 (2020).
- 27. J. Korenaga, Thermal cracking and the deep hydration of oceanic lithosphere: A key to the generation of plate tectonics? *J. Geophys. Res.* **112**, B05408 (2007).
- 5 28. M. Baes, R. J. Stern, S. Whattam, T. V. Gerya, S. V. Sobolev, Plume-Induced Subduction Initiation: Revisiting Models and Observations. *Front. Earth Sci.* **9**, 766604 (2021).
 - 29. R. I. Citron, D. L. Lourenço, A. J. Wilson, A. G. Grima, S. A. Wipperfurth, M. L. Rudolph, S. Cottaar, L. G. J. Montési, Effects of Heat-Producing Elements on the Stability of Deep Mantle Thermochemical Piles. *Geochemistry, Geophysics, Geosystems.* 21, 1–17 (2020).
- 30. A. N. Halliday, R. M. Canup, The accretion of planet Earth. *Nat Rev Earth Environ.* **4**, 19–35 (2022).
 - 31. L. Moresi, S. Quenette, V. Lemiale, C. Mériaux, B. Appelbe, H.-B. Mühlhaus, Computational approaches to studying non-linear dynamics of the crust and mantle. *Physics of the Earth and Planetary Interiors.* **163**, 69–82 (2007).
- 32. Y. Li, M. Gurnis, A simple force balance model of subduction initiation. *Geophysical Journal International.* **232**, 128–146 (2022).
 - 33. B. R. Hacker, G. A. Abers, S. M. Peacock, Subduction factory 1. Theoretical mineralogy, densities, seismic wave speeds, and H ² O contents: SUBDUCTION ZONE MINERALOGY AND PHYSICAL PROPERTIES. *J. Geophys. Res.* **108** (2003), doi:10.1029/2001JB001127.
- 34. E. Tan, M. Gurnis, Metastable superplumes and mantle compressibility. *Geophysical Research Letters*. **32**, 1–4 (2005).

- 35. J. O'Neil, R. W. Carlson, D. Francis, R. K. Stevenson, Neodymium-142 Evidence for Hadean Mafic Crust. *Science*. **321**, 1828–1831 (2008).
- 36. R. W. Carlson, M. Garçon, J. O'Neil, J. Reimink, H. Rizo, The nature of Earth's first crust. *Chemical Geology*. **530**, 119321 (2019).
 - 37. Y. Miyazaki, J. Korenaga, A wet heterogeneous mantle creates a habitable world in the Hadean. *Nature*. **603**, 86–90 (2022).

Acknowledgments

We thank M.M. Li, W. Mao, Y. Miyazaki for fruitful discussions. We also acknowledge use of the Anvil supercomputer at Purdue University supported by the NSF ACCESS program.

5 Funding

10

15

25

30

Q. Yuan acknowledges support from the O.K. Earl Postdoctoral Fellowship at Caltech. This work is supported by National Science Foundation NSF award 2049086.

Author contributions

Q.Y conceived the project and performed all experiments. All authors contributed to the analysis of the models and writing of the manuscript.

Competing interests

Author declare no competing interests.

Data and materials availability

All data and parameters are available in the main text or the supplementary materials.

Supplementary Materials:

20 Materials and Methods

Figures S1-S9

Table S1. Model parameters used in the numerical experiments.

References

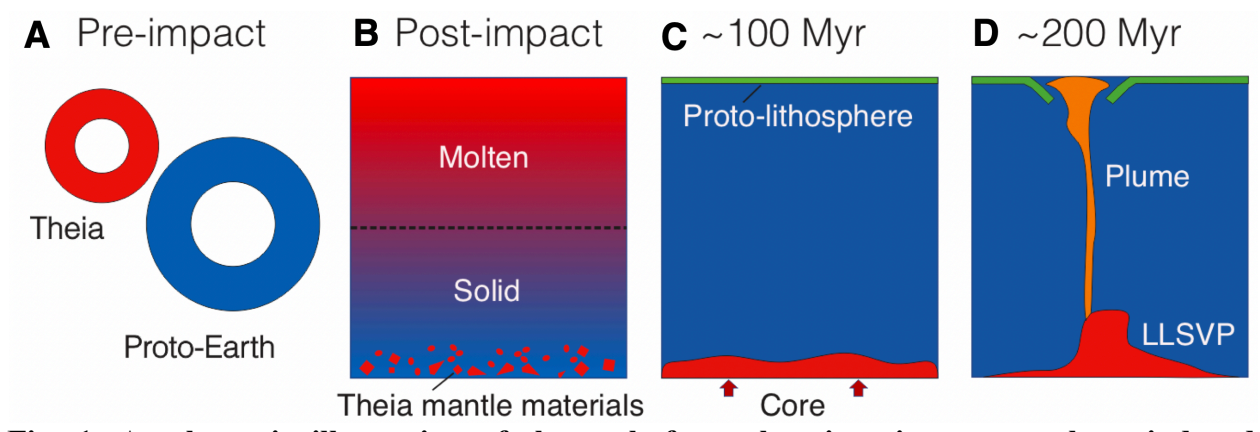


Fig. 1. A schematic illustration of the path from the giant impact to plume-induced subduction in the early Hadean. A canonical Moon-forming giant impact (A) leads to a two-layered mantle structure (B) [10, 11]. After solidification of the upper magma ocean (~100 Myr, [14]) a proto-lithosphere formed [15] (C), which was then destabilized and segmented by impact of a mantle plume from an LLSVP made of the Theia mantle remnant (D).

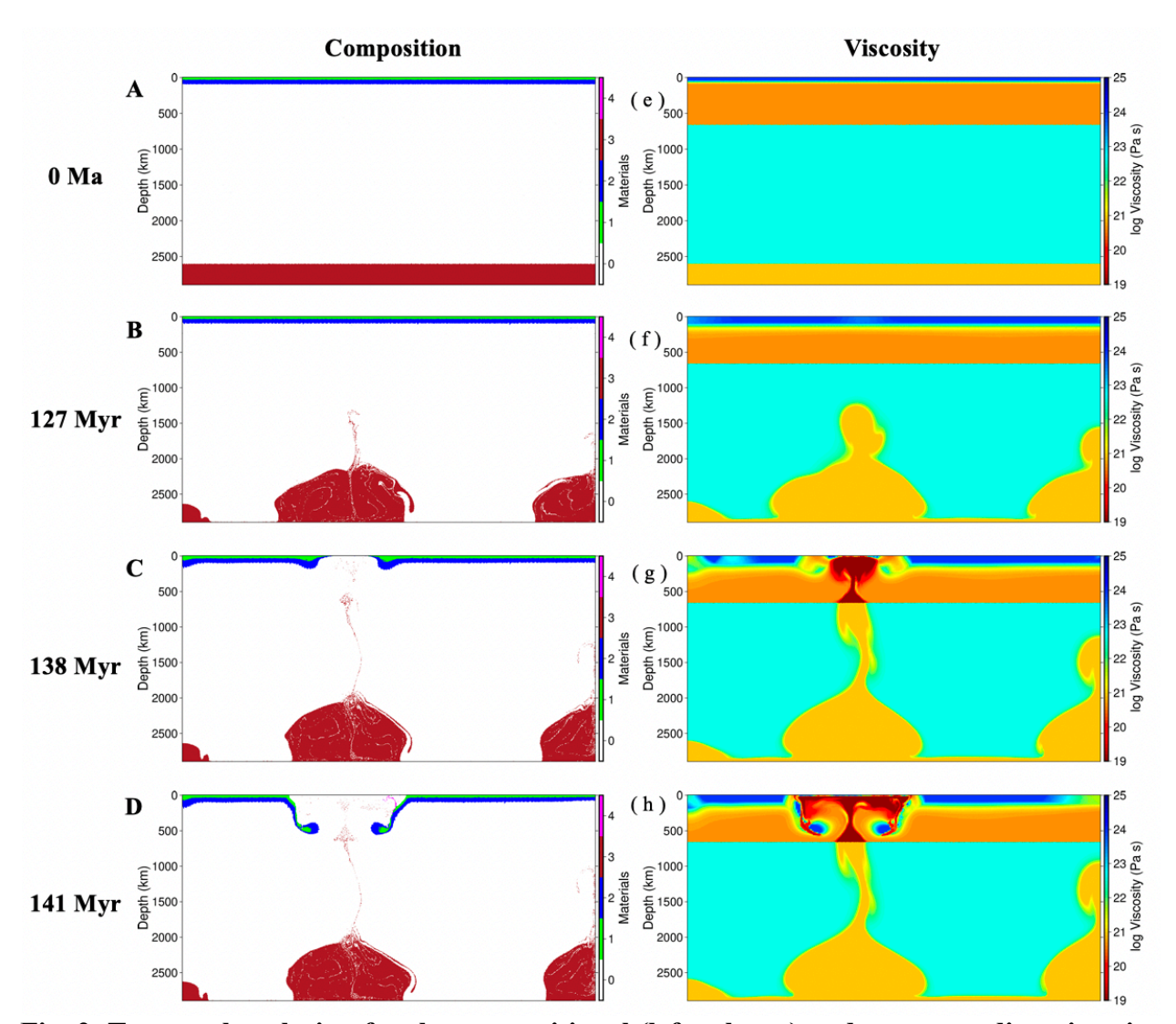


Fig. 2. Temporal evolution for the compositional (left column) and corresponding viscosity (right column) field of the reference case showing a LLSVP-sourced plume induced subduction initiation. (A) Initial set up of the model; (B) Plume rising from the LLSVP at 127 Myr; (C) Plume penetrates the lithosphere at 138 Myr; (D) Slab retreat and melting of crust at 141 Myr. In panel A, materials 0 to 4 are mantle, crust, lithosphere, LLSVP pile and molten materials.

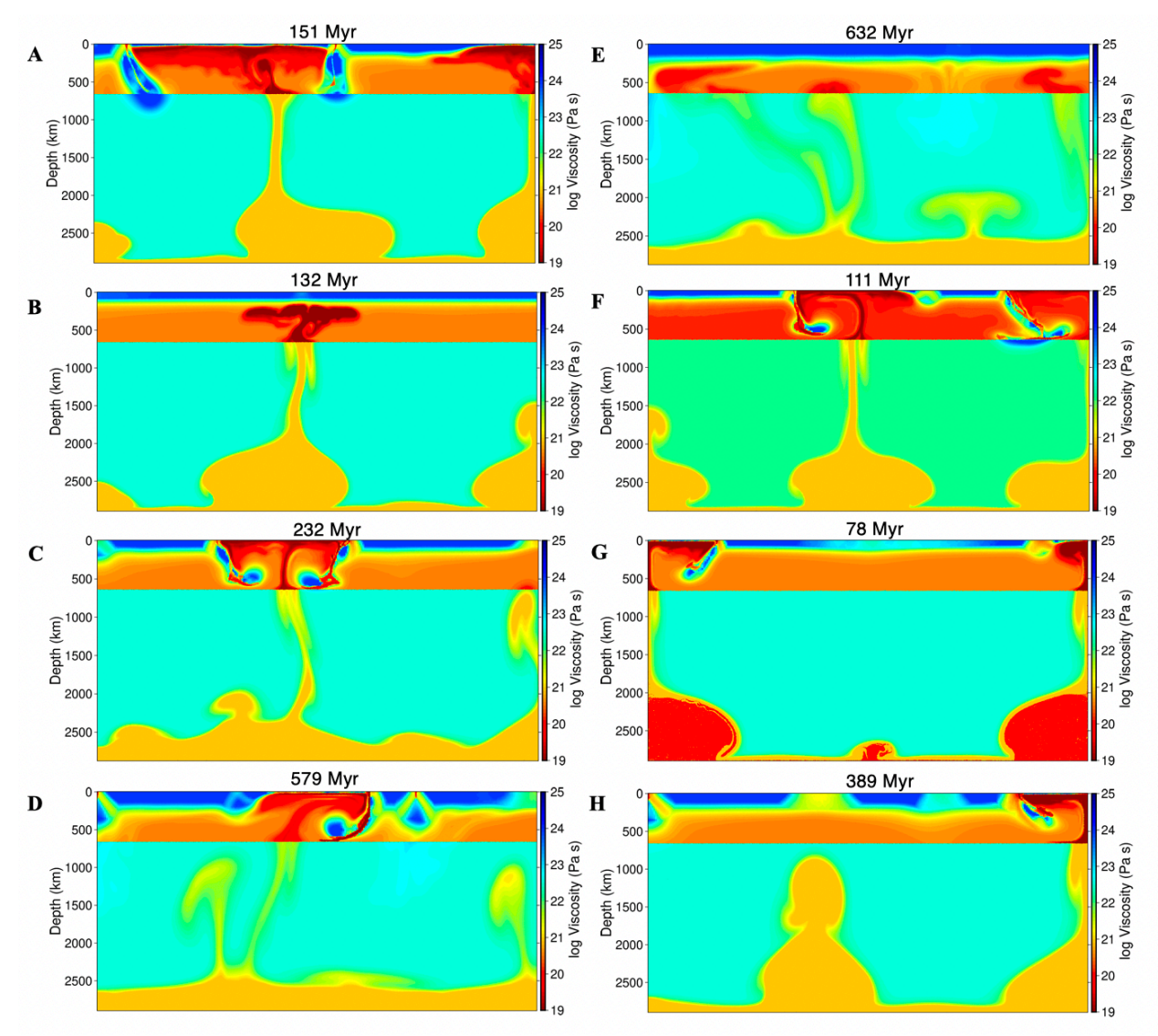


Fig. 3. Snapshots of viscosity field of eight representative cases showing a LLSVP-sourced plume induced subduction initiation when the CMB temperature is high and surface yield stress is small. In panel (A) and (B), the lithosphere yield strength is 70 and 100 MPa, respectively. Panel (C) and panel (D) has a CMB temperature that is 4,273 K and 2,723 K, respectively. Panel (E) has the same low CMB temperature as panel (D) but with a slightly larger lithosphere strength. In panel (F), the background mantle temperature is 373 K higher than the reference. In panel (G), the pile materials has a compositional-dependent viscosity that is 10 times smaller than the reference case. Panel (H) shows the results of a case which reference viscosity is five time larger compared to that in the reference case. In all results, the lithosphere can get subducted in a range of 70–580 Myr except when the lithosphere is sufficient strong (panel B) and CMB temperature is low (panel E).

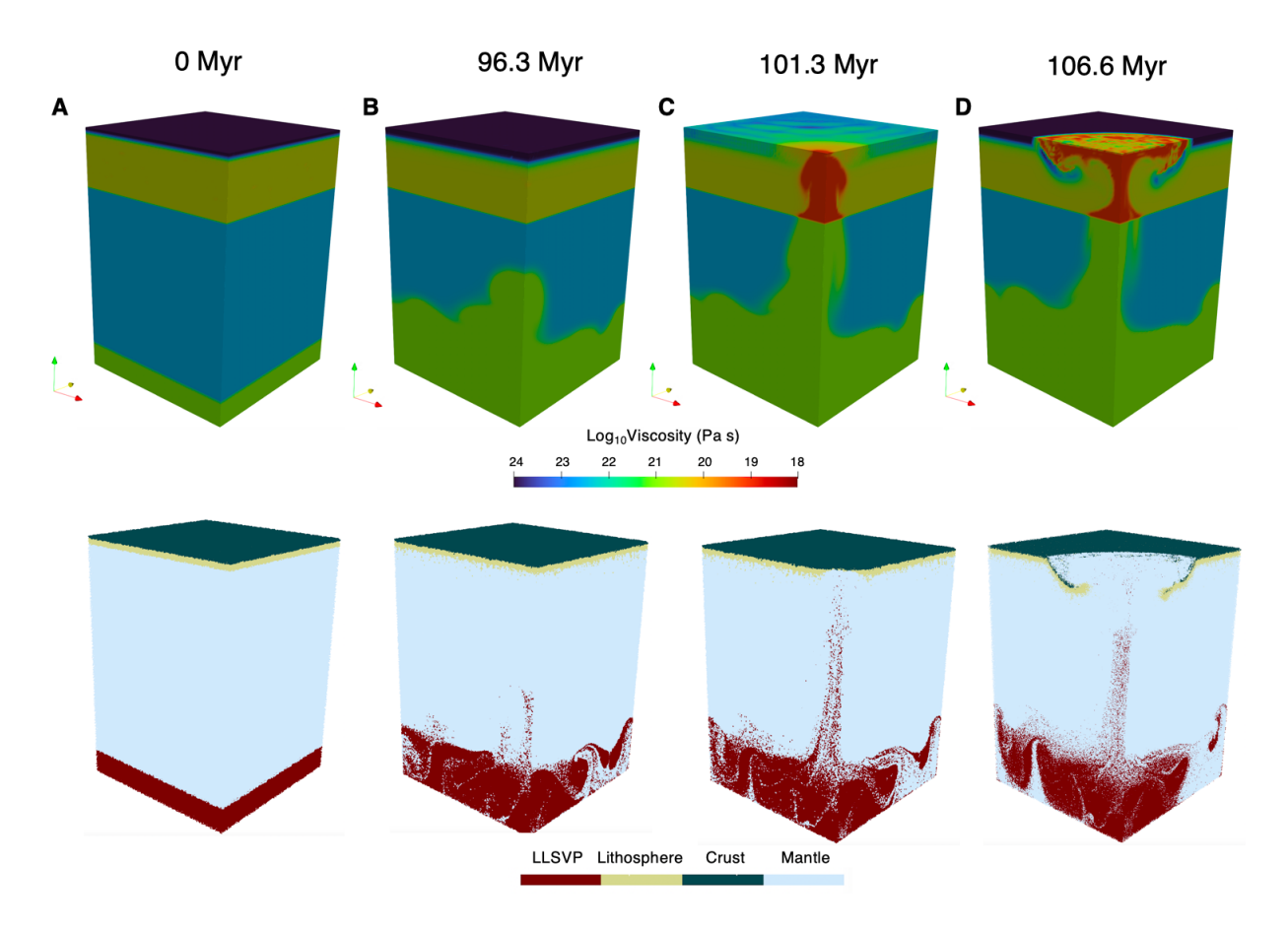


Fig. 4. Temporal evolution for the viscosity (upper row) and compositional (lower row) field of the 3D reference case showing a LLSVP-sourced plume induced subduction initiation. (A to D) Model snapshots at 0 Myr, 96.3 Myr, 101.3 Ma, and 106.6 Myr, respectively.

MATERIALS AND METHODS

We perform whole-mantle convection model in both 2D and 3D using *Underworld2*, an opensource, particle-in-cell, finite element code (31), to investigate how LLSVP-sourced mantle plume may give rise to the first subduction in the Hadean. Our 2D Cartesian models are intended to systematically explore the plume-induced subduction initiation and related parameters, whereas 3D Cartesian geometry is used to verify the main findings we acquired from our 2D results.

Governing equations

5

10

15

20

25

30

Our 2D thermomechanical models were calculated using the *Underworld2* geodynamic framework to solve the conservation equations of mass, momentum, and energy:

$$\nabla \cdot u = 0 \quad (1)$$

$$\nabla \cdot \sigma' - \nabla P + \rho g = 0 \quad (2)$$

$$\rho c_p \left(\frac{\partial T}{\partial t} + u \cdot \nabla T \right) - \nabla \cdot k \nabla T - H = 0. \quad (3)$$

where u is velocity, σ' is deviatoric stress, P is pressure, ρ is density, g is gravitational acceleration, c_p is heat capacity, k is thermal conductivity and H is heat production.

Material description

Computations with both viscoplastic and viscoelasto-plastic rheologies are performed to investigate its effect of subduction initiation. An incompressible Maxwell-rheological model is adopted to reflect viscoelastic behavior as below.

$$\dot{\varepsilon} = \frac{1}{2K_e} \, \dot{S}_{ij} + \frac{1}{2\eta} S_{ij} \quad (4)$$

where $\dot{\varepsilon}_{ij}$ is the strain rate tensor, S_{ij} is the deviatoric part of the stress tensor, \dot{S}_{ij} is the Jaumann corotational rate of S_{ij} , K_e is the shear modulus for elasticity, and η is the viscosity.

Non-Newtonian and temperature-dependent rheology is specified by:
$$\eta(T,\dot{\varepsilon}) = \eta_0 e^{\frac{E}{nRT} - \frac{E}{nRT_0}} \left(\frac{\dot{\varepsilon}}{\dot{\varepsilon}_0}\right)^{\frac{1-n}{n}} \ (5)$$

where E is the activation energy, R is the idea gas constant and n is the non-Newtonian viscosity, the materials yields by imposing an upper limit on the stress, thus the effective viscosity becomes

$$\eta_{eff} = \min(\eta(T, \dot{\varepsilon}), \frac{\tau_y}{\dot{\varepsilon}_{II}})$$
 (6)

where τ_v is the yield stress and $\dot{\varepsilon}_{II}$ is the square root of the second invariant of strain rate tensor. The effective viscosity is restricted to the range between 10^{18} Pa s and 10^{24} Pa s. The yield stress follows the Drucker-Prager yielding criteria with an upper cut-off.

$$\tau_{v} = \min (C + \mu_{v} p, \tau_{v0})$$
 (7)

Similar to previous studies (32), weakening processes are approximated by reducing the yield stress with plastic strain, following a two-stage process: Prior to a strain saturation, C and μ_{γ} linearly decreases with accumulation of plastic strain ϵ_{P} , and afterwards τ_{γ} remains constant.

$$\tau_{y} = \begin{cases} C + \mu_{y} p, & \epsilon_{P} \leq \epsilon_{P0} \\ \tau_{yf}, & \epsilon_{P} > \epsilon_{P0} \end{cases}$$
 (8)

Where ϵ_{P0} is the reference plastic strain that determines the rate of weakening. C and μ_y are cohesion and friction coefficient, $C = (\tau_{yf} - C_0) \frac{\epsilon_P}{\epsilon_{P0}} + C_0$ and $\mu_f = \mu_{y0} - \mu_{y0} \frac{\epsilon_P}{\epsilon_{P0}}$.

Three materials are present within the model domain: a 30-km-thick mafic crust on top that can metamorphose to eclogite at depth (33); and depth-dependent density of LLSVPs materials (34), and background mantle for the remainder of the model. Although geochemical observations require the existence of a differentiated mafic crust at 4.4-4.5 Ga (35), the composition of the earliest crust remains uncertain, as none of the rocks currently present on the Earth's surface clearly represent it. It is expected that the earliest crust could either be peridotitic resulting from a quenching process of a magma ocean (36), or iron-rich dense crust from fractional crystallization of a deep magma ocean (37). In this study, we generally neglect chemical density difference in the mafic crust, but we also verified our findings by considering scenarios with a chemically-buoyant basaltic crust in both 2D (Fig. 3H) and 3D (Fig. S9).

2D Model setup

5

10

15

20

25

30

35

Most 2D model domain is 5780 × 2890 km with 256 × 128 linear, quadrilateral elements, with 30 Lagrangian particles in each element. We have verified the validity of 2D results with a higher-resolution grid of 512 × 256 elements for the same model domain, and in longer aspect ratio of 14450 × 2890 km with 640 × 128 elements. A free-slip boundary condition is applied to both vertical and horizontal boundaries of the model domain. The temperature at the upper boundary is maintained at 273 K, and the bottom boundary is fixed at a varying temperature (6,273 K down to 2,773 K) to test its effect on plume-induced subductions. The maximum yield strength of the lithosphere is varied between 40 MPa to 100 MPa, consistent with estimation for proto-lithosphere in early Earth. More than 100 calculations have been performed, varying the boundary condition (reflective and periodic), lateral extent of the model domain (2,800, 5,780 or 14,450 km), CMB temperature (2,773–6,273 K), age (thickness) of the lithosphere (25–200 Ma), maximum yield stress of the lithosphere (40–100 MPa), weakening rate (1–4), the density of the basaltic crust (3,000 to 3,300 kg/cm³), and various density and rheologies of the calculations. Other parameters are listed in Table S1.

Because a thermodynamic model that can reliably predict the P-T relations of the solidus and liquidus for these unknown earliest crustal compositions is not currently available, we used a crude first-order approximation that the top 10 km mafic rocks to melt instantaneously and completely above temperatures of 1,273 K. Because we are primarily interested in how plume

inducted subduction, we do not expect sophisticated melting of crustal materials significantly alter our model outcomes.

3D Model setup

Models consist of a 3D Cartesian domain 2,890 km deep, $2,000 \times 2,000$ km horizontally. We use a resolution of $128 \times 80 \times 80$ elements with a uniform grid spacing in each coordinate direction. Each element initially has 10 material points randomly located in each element. Free slip conditions are applied to the all boundaries. These 3D results were used to verify our 2D results, hence except having an extra dimension, the properties of the materials are the same as that in the two-dimensional model.

SUPPLEMENTARY MATERIALS

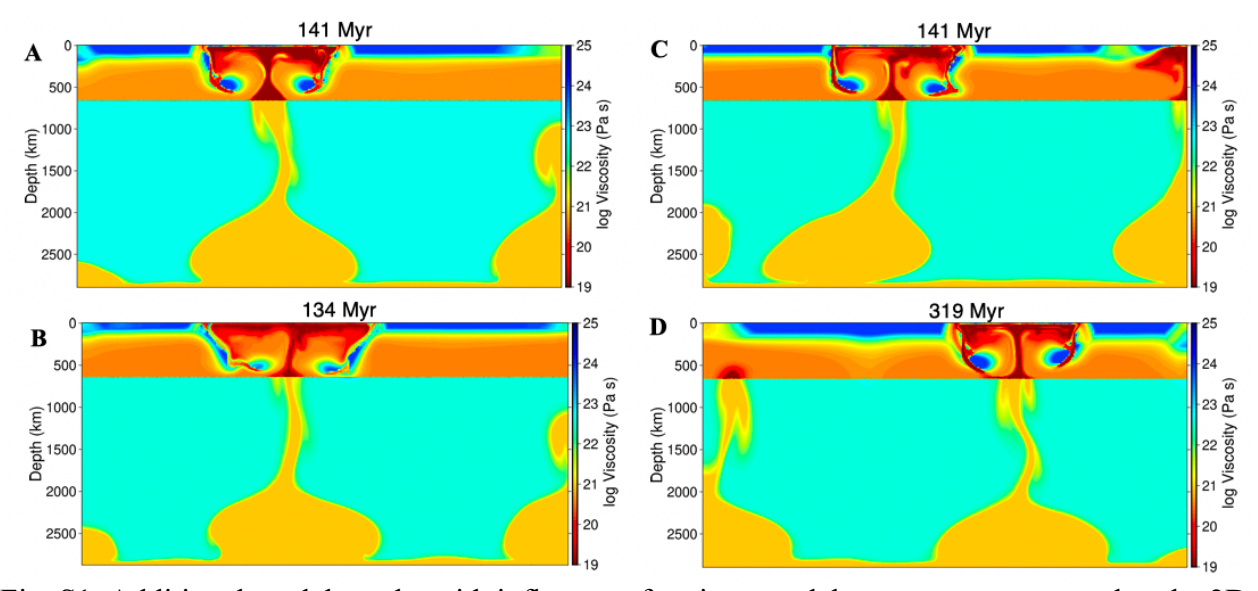


Fig. S1. Additional model results with influence of various model parameters compared to the 2D reference case. Panel **A** incorporates a higher temperature-dependent viscosity, while panel **B** includes a chemically buoyant basaltic crust that is 10 kilometers thick and has a density of 3,000 kg/cm³. Panel **C** demonstrates the case has a relatively less dense LLSVP materials, while panel **D** showcases a lower initial temperature of the LLSVP.

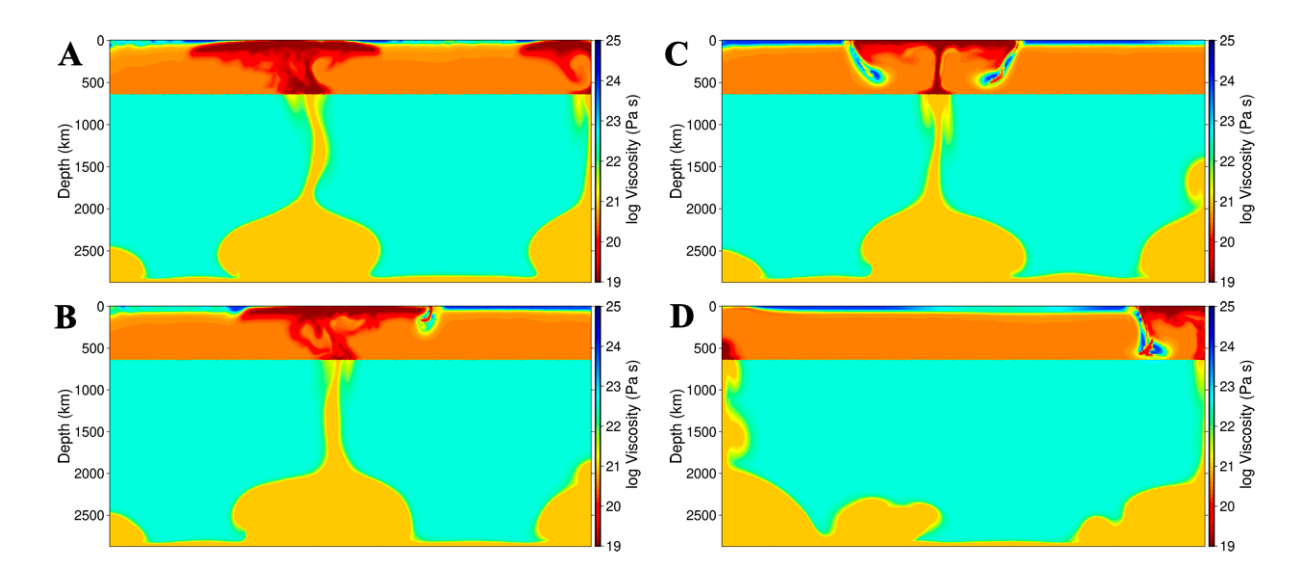


Fig. S2. Additional models showing the effect of different ages of the initial lithosphere. From panel A to D, the lithosphere age is initially 25 Myr, 50 Myr, 75 Myr and 100 Myr, respectively. Note that the plume did not induce subduction for the case with a 25-Myr-old lithosphere.

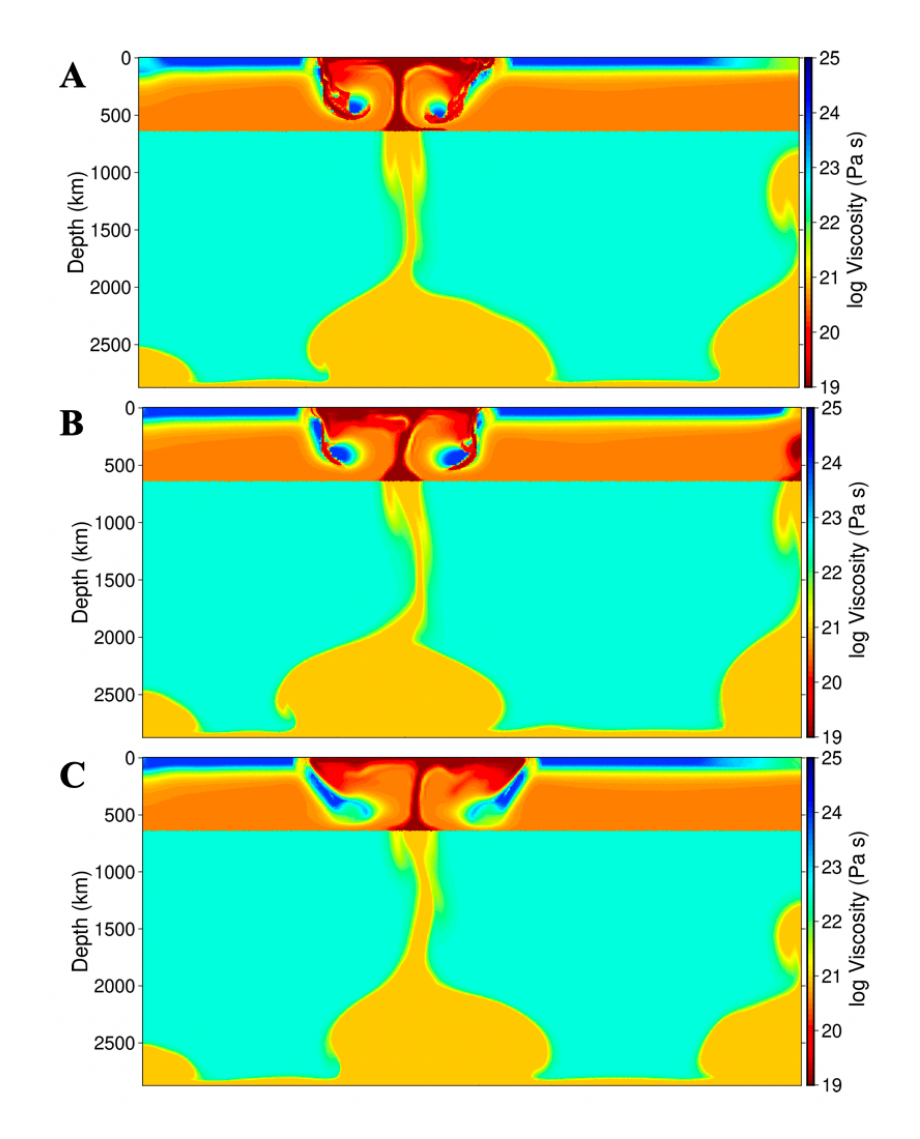


Fig. S3. Additional models showing the effect of different reference plastic strain. From Panel A to C, the reference plastic strain is respectively 1, 2, and 4.

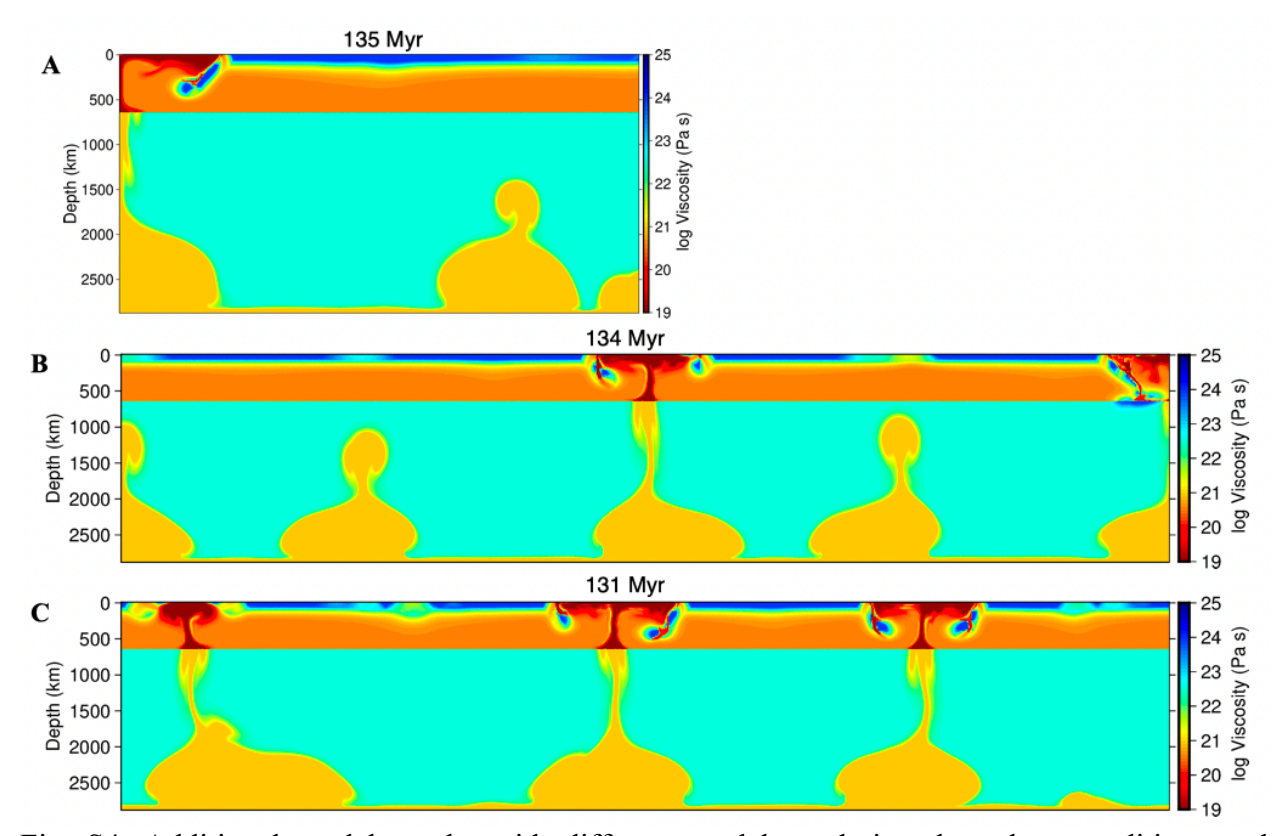


Fig. S4. Additional model results with different model resolution, boundary conditions and different aspect ratio of model (5:1). Panel A has a double resolution compared to the 2D reference case. Panel B has a reflective side boundary condition while panel C has a periodic boundary condition with aspect ratio of 5.

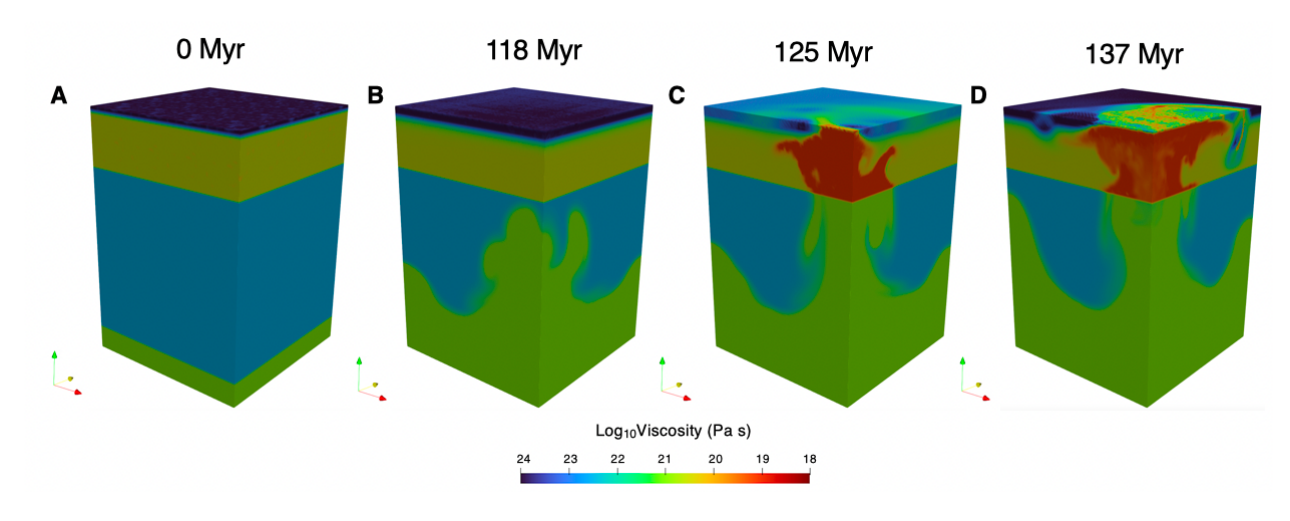


Fig. S5. Temporal evolution for the viscosity field of the 3D case with a higher yield strength (60 MPa) of the lithosphere showing a segment of lithosphere was broken and subducted.

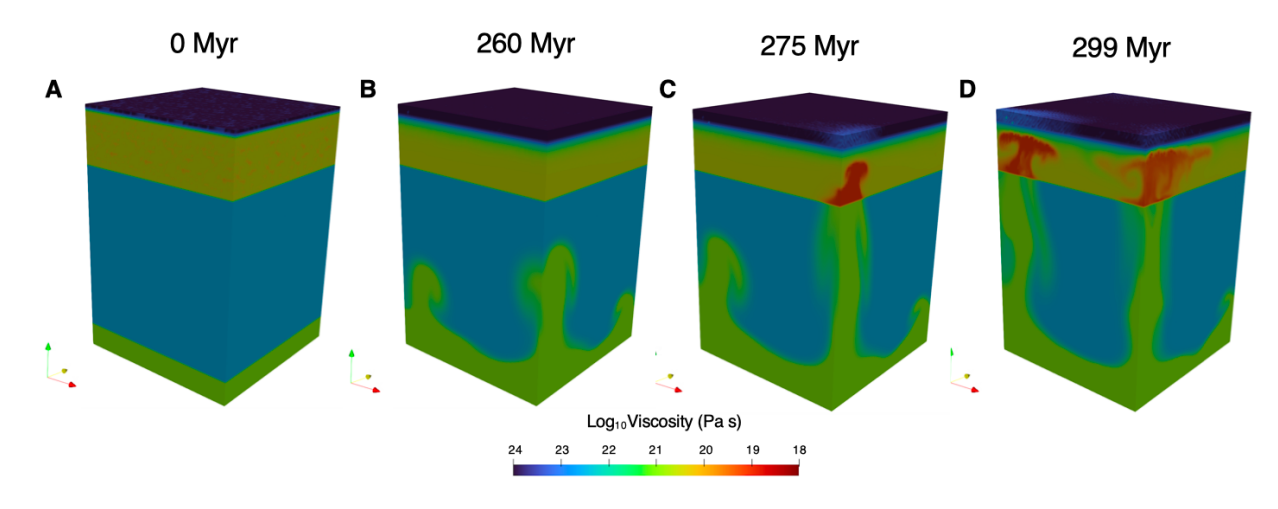


Fig. S6. Temporal evolution for the viscosity field of the 3D case with a CMB temperature of 4,273 K showing plume failed to induce subduction.

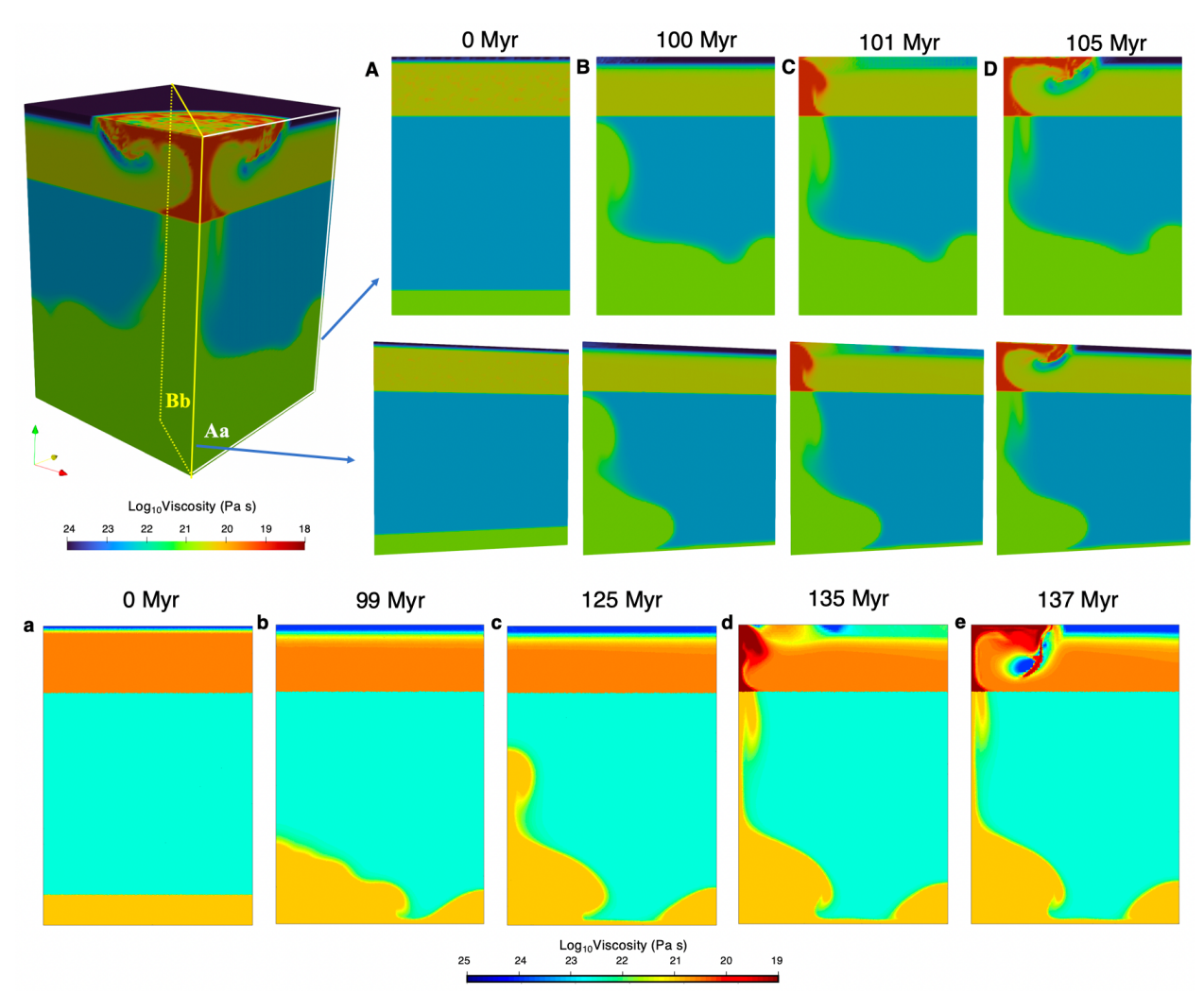


Fig. S7. Comparison between the reference 3D case with a 2D case. The bottom row shows temporal evolution of the 2D case and the top two rows show the temporal evolution from two different slices from the 3D case. The comparison between different dimensions suggest the boundary effect on increasing plume rising speed in 3D is reduced compared in 2D. In our 2D models, we do not find that the boundary effect significantly benefits the capability for plume-induced subduction by comparing cases with a periodic and reflective boundary condition, respectively (fig. S2).

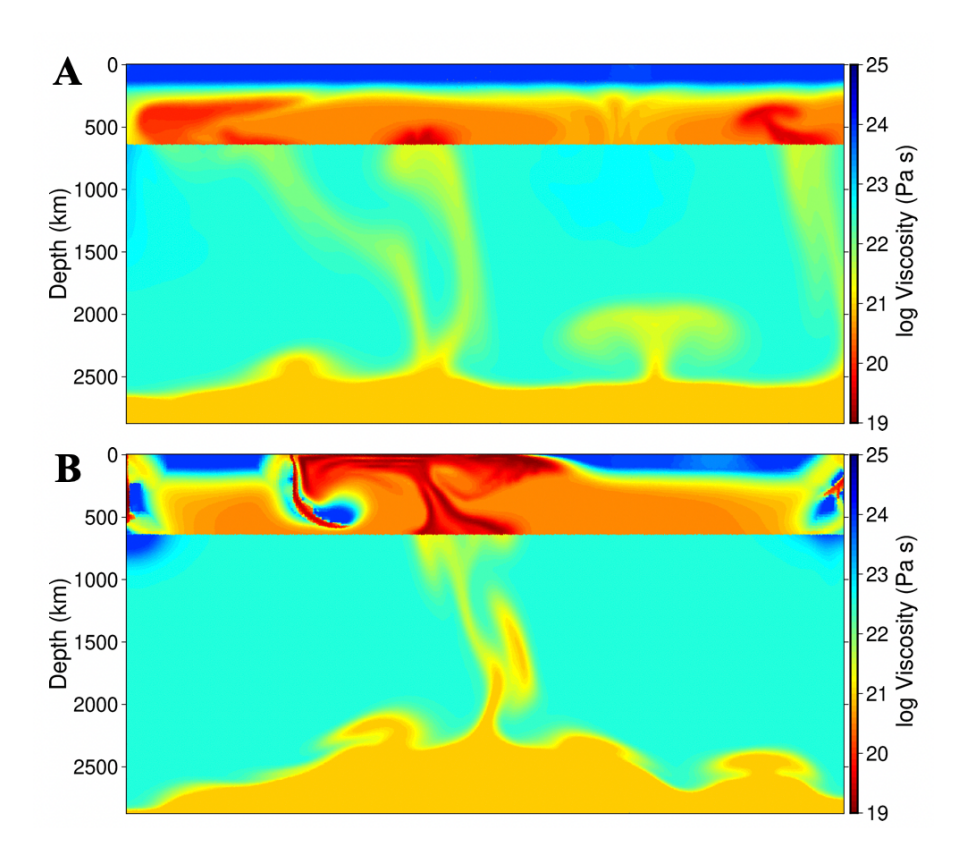


Fig. S8. A comparative analysis revealing the enhanced subduction initiation potential of plumes from a heat-producing element enriched LLSVP in the presence of a low-temperature CMB. Panel A shows the same model in Figure 3E, where plumes failed to induce subduction initiation with a CMB temperature of 2,750 K. Panel B has the same parameter except the LLSVP materials is enriched in heat-producing elements, which leads to a dimensional heating rate is 5.54×10^{-7} W·m⁻³.

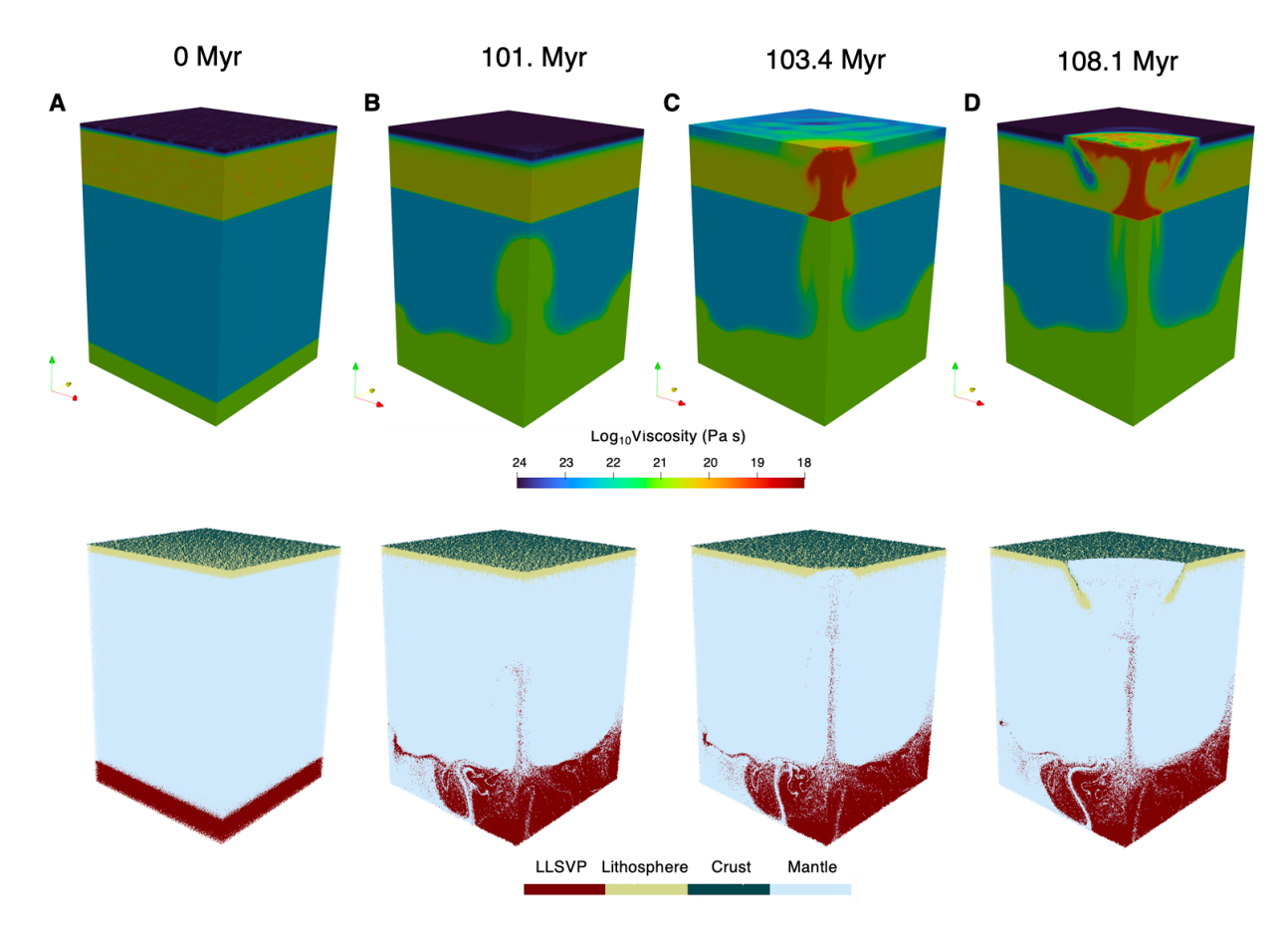


Fig. S9. Temporal evolution for the viscosity (upper row) and compositional (lower row) field of the 3D reference case with a chemically-buoyant crust.

Table S1. Model parameters used in the numerical experiments.

| Symbol | Definition | Value |
|-----------------------|----------------------------------|--|
| D | Mantle thickness | 2,890 km |
| α | Thermal expansivity | $3 \times 10^{-5} \text{ C}^{-1}$ |
| k | Thermal diffusivity | $1 \times 10^{-6} \text{ m}^2 \cdot \text{C}^{-1}$ |
| n | Non-Newtonian exponent | 3 |
| E | Activation energy | $540 \mathrm{~kJ~mol^{-1}}$ |
| η_{max} | Maximum viscosity | 10^{25} Pa s |
| η_{min} | Minimum viscosity | $10^{18} \mathrm{Pa} \mathrm{s}$ |
| μ | Shear modulus | 3×10^{10} Pa s |
| $\dot{\mathcal{E_0}}$ | Reference strain rate | $10^{-15}\mathrm{s}^{-1}$ |
| T_{0} | Surface temperature | 273 K |
| T_1 | Mantle temperature | 1,673 K |
| T_{CMB} | Core-mantle boundary temperature | 2,773K to 6,273 K |
| $	au_{y0}$ | Maximum yield stress | 40 to 100 MPa |
| $	au_{yf}$ | Minimum yield stress | 3 MPa |
| $arepsilon_{P0}$ | Reference plastic strain | 1 to 4 |
| h | Mafic crust thickness | 30 or 10 km |
| C_0 | Initial cohesion | 44 MPa |
| μ_{y0} | Initial friction coefficient | 0.6 |
| ho | Reference density | $3,300 \text{ kg/m}^3$ |
| $ ho_b$ | Basaltic crust density | $3,000 \text{ kg/m}^3$ |